A MODELLING FRAMEWORK FOR THE CALCULATION OF STRUCTURAL LOADS FOR FATIGUE LIFE PREDICTION IN HELICOPTER AIRFRAME COMPONENTS

R.J.J. Bakker, M.J. Bos, N. Münninghoff, J.H. van Tongeren, H. van der Ven,
National Aerospace Laboratory NLR
P.O. Box 90502, 1006 BM Amsterdam, the Netherlands

Abstract

A modelling framework for determining structural dynamic loads in airframe components has been developed. This paper addresses the flight dynamics and structural modelling tools of the framework and presents the results validations. Validation of the calculated component strains has been done by means of comparison with strain gauge measurements on the aft-pylon engine frame during scheduled operational flights. Results show a good agreement for the 3/rev vibrations of the component. Vibrations at higher frequencies are under predicted. Trend analyses provides insight in weight, flight speed and altitude dependencies. The proposed framework is capable of calculating structural dynamic loads of an airframe component in a relatively simple and cost-effective way.

1. INTRODUCTION

Present day maintenance programs for helicopters are often schedule based which means that a helicopter component is replaced after a predetermined number of flight hours. Future maintenance procedures aim at maintenance 'on condition' which means that a component is replaced when it is degrading or when the actual operational life is reached. A thorough and reliable knowledge of the exerted loads on the component for all flight conditions and the consequent effect on fatigue life is essential for the development of such maintenance procedures. NLR, in cooperation with the Royal Netherlands Air Force (RNLAF), has started an extensive flight data acquisition program to enable a fleet wide assessment of the fatigue loads in relation to the usage of the aircraft. Good results have been achieved in determining the relative fatigue load for different missions on the basis of measurements.

Complementary to the measurement program a project commissioned by the RNLAF was set up aiming at the prediction of helicopter component fatigue loads. Calculating vs. measuring the structural loads offers advantages in terms of flexibility in the component choice and the desired flight conditions (including undesirable ones). Component structural loads that are difficult to measure can be addressed and the calculation process does not interfere with helicopter operations.

Calculation of a structural dynamic load sequence in an arbitrary component of a detailed airframe with present day finite-element programs coupled with CFD tools would nowadays still require too much computational effort. The proposed framework is based on using a chain of relatively simple physics modelling tools with encouraging results.

In the next section the modelling framework is described, followed by the results of the validation exercises. Conclusions and recommendations are presented in the final sections.

2. MODELLING FRAMEWORK

The modelling framework consists of a set of computational tools for structural dynamics (for a coarse fuselage model and a detailed airframe component model) rotorcraft flight dynamics and fatigue loads prediction. The methodology is based on work that has been presented by Lang and Centolanza [1] and is based on the following principles:

1) A relatively coarse dynamic airframe model is used to perform a modal analysis. The resultant natural frequencies and mode shapes of the airframe are input for the flight dynamics and rotor-airframe response computation.

2) The modal properties of the coarse airframe model are used by the comprehensive rotorcraft flight dynamics code to calculate the rotor loads and airframe dynamic response for the desired flight condition.

3) The deformations of the coarse airframe model are interpolated onto a detailed finite element model of the chosen component and the resulting stress is determined.

4) A fatigue analysis can be performed using the local stress sequence to determine the fatigue load of the component for a defined mission.

In the following sections the different modules are discussed in more detail.

©DGLR 2009

2.1. Airframe structural computations

The coarse airframe structural model consists of plates, frames and stiffeners. A NASTRAN computation provides the natural frequencies and modes shapes of the airframe. The airframe stiffness properties are tuned to match the dynamic characteristics that were found in open literature. The Chinook aft pylon engine frame was chosen for the study of the dynamic behaviour and fatigue analysis.

2.1.1. Airframe structural model

The fuselage model is a shell model that captures the most essential components of the fuselage structure. The dimensions are derived from a limited set of drawings and photographs. For an impression of the model, see FIG. 1.

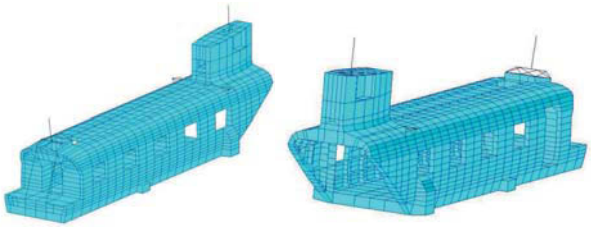

FIG. 1. Front and rear view of the shell finite element model of the CH-47D

The resulting model is a simplification in four aspects: geometry, structural detail, shell properties (thickness and material) and mass properties, which are described in more detail below

The geometry is simplified in the sense that the fuselage cross-section is assumed to be constant over the full length of the fuselage. This is obviously not correct for the nose and tail regions. However, these geometric aspects do not have a significant impact on the overall model vibration behaviour. For a detailed stress analysis in the nose and tip regions the model geometry would need to be refined. Given the location of the component of interest (aft flange of the rear pylon frame, see FIG. 9) this is not necessary.

The level of structural detail can be classified as “coarse”. The model contains only those structural components that are essential for the transfer of loads. All other components (covers, hatches, etc.) are ignored. The heavy items: rotor heads and engines are attached to the proper fuselage locations using rigid beam connections. The whole windshield region is reduced to the only two essential components: two window posts simplified as beams. The model does contain stringers but only half the number in the actual airframe. The stringer properties are combined. Currently the fuel tanks and the ramp are not modelled. These may have influence on the fuselage stiffness. However, their attachment to the fuselage requires a study and tuning of the actual effective load paths. This effort is significant, where the effects may be of second order for the stress of the aft pylon. Therefore this was postponed to a later stage of this project.

The thickness of all skin/plate type components is uniform across the entire fuselage. All skin panels have the same thickness. All fuselage frames have the same thickness. The stringers have approximately correct individual cross-section areas, but have constant area over the entire fuselage length. All components are assumed to be made of aluminium with 2024 alloy properties.

The fuselage mass distribution is presented TAB 1 (taken from [5]). The model places concentrated masses at each fuselage frame. Each mass is placed on the fuselage centre line. It is attached to the nodal points on the intersection of the frame plane and the fuselage skin. This is illustrated in FIG. 2 and FIG. 3. The connection is made using a NASTRAN construct called RBE3 that assigns the average of all skin displacements to the central point. In the opposite direction a load on the central point is distributed over the skin points. The most important aspect of RBE3 constructs is that they do not add stiffness to the model. That is, the frames are still flexible. The heavy mass items are attached to the nearby structure in a manner consistent with the real structure:

The hub masses are attached to the top of the rotor shafts. The engines are attached to frames at fuselage stations 482 and 502. The APU, cockpit and electronics mass items are added to the concentrated masses at the centre line. Apart from the concentrated masses for the rotors, engines etc, the remaining mass are uniformly distributed over the airframe. The 27000 lb OWE mass was transformed to other mass levels by scaling the concentrated masses along the fuselage centre line. The contributions from heavy mass items at these points were not affected.

OWE mass		27,000 lb
Heavy items		10,150 lb
1. fwd rotor	2,100 lb	
2. aft rotor	2,100 lb	
3. engines	2,400 lb	
4. APU (est.)	1,100 lb	
5. cockpit (est.)	1,300 lb	
6. electronics	1,000 lb	
Remaining mass		16,850 lb

TAB 1. Mass data collected from various sources

©DGLR 2009

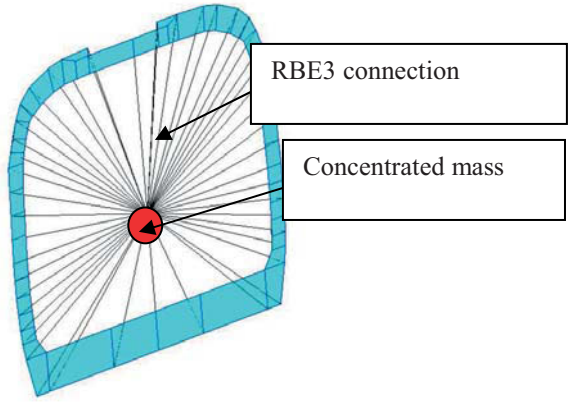

FIG. 2. Typical concentrated mass on the centre line of the helicopter fuselage at a frame station.

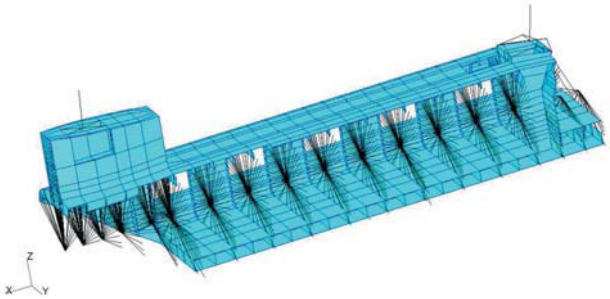

FIG. 3. Cut-away plot of the fuselage model exposing the RBE3 constructs (black spider webs) used for concentrated mass attachment to the frame/skin.

The modal analysis of the unsupported fuselage model results in a series of resonance frequencies and modes. Only the lowest resonance frequencies can be expected to be of some significance at this stage of the project. The results for the first three flexible modes are presented in FIG. 4. TAB 2 presents the tuned frequencies compared to the model as presented in [6].

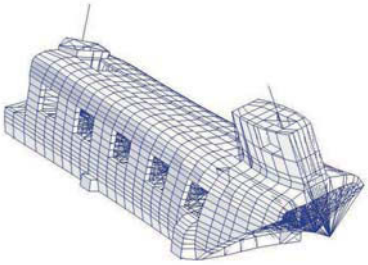

(a) 1st flexible mode at 6.36 Hz (Boeing: 6.36 Hz; 1st lateral – aft pylon lateral)

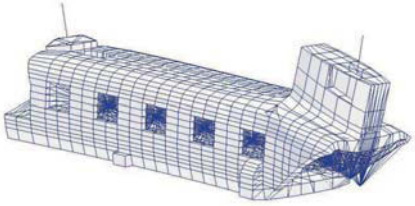

(b) 2nd flexible mode at 6.81 Hz (Boeing: 7.52 Hz, 1st vertical – aft pylon longitudinal)

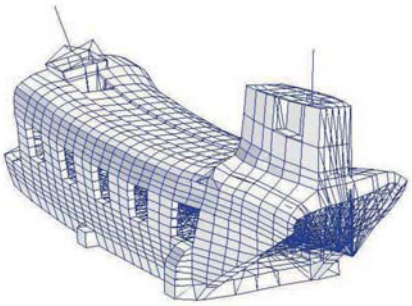

(c) 3rd flexible mode at 11.62 Hz (Boeing: 12.89 Hz, 2nd lateral – fwd pylon lateral)

FIG. 4. Selected flexible modes for the tuned 27000 lb model

Mode	Frequency (Hz)		Mode description
	Boeing	NLR tuned	
1	6.36	6.36	1st lateral, aft pylon lateral
2	7.24	*	Engine lateral yaw – out of phase
3	7.52	6.81	1st vertical, aft pylon longitudinal
4	8.24	*	Engine lateral yaw – in phase
5	11.80	11.94	2nd vertical – pylon longitudinal
6	12.89	11.62	2nd lateral – fwd pylon lateral
7	13.81	13.83	3rd lateral – pylon lateral in phase

* = mode is not predicted by the NLR model because of the assumed rigid engine attachment

TAB 2. Comparison of published Boeing results and the tuned NLR 27000 lbm model results.

The aeromechanics model already contains a mass at the hub location. It was determined that the hub mass in the fuselage model has to be reduced from 2100 lb to 400 lb in order to prevent duplication. This mainly affects the resonance frequencies (see TAB 3 for examples). Mode shapes are very similar for the three aircraft weights.

2.1.2. Component model

The fuselage model mesh has been refined at the crown

©DGLR 2009

of frame 482 thus providing enough detail to capture the actual location of strain gauges in this region. Stress results are derived from the whole fuselage model with refined mesh at FS 482. FIG. 5 illustrates the mesh refinements in the region of strain gauge 2. No separate component model is used in the present study.

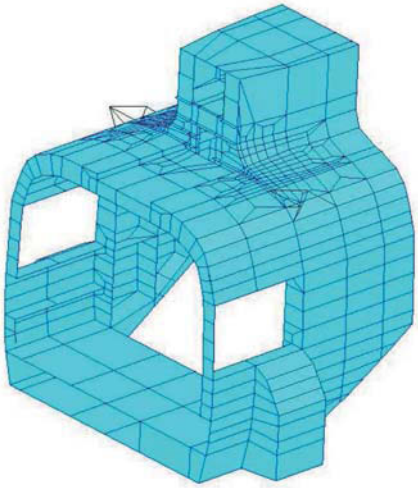

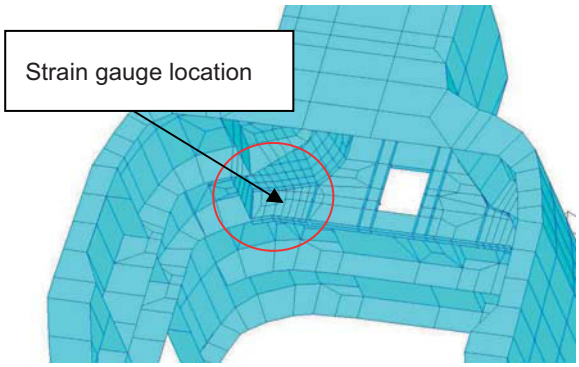

Front view from above and rear view from below

FIG. 5. Views of the refined mesh model near the FS482 frame crown

The dynamic fuselage properties used in the aeromechanics model are derived from the fuselage model including this refinement.

Frequency results for the refined fuselage model at various aircraft weights are presented in TAB 3. Note that frequencies have changed significantly by weight changes and the reduction of hub mass (compare with TAB 2). The mode shapes remain very similar.

Mode	Frequency (Hz)			Mode description
	27k lb	37k lb	48k lb	
1	8.37	6.98	6.03	1st lateral, aft pylon lateral
3	10.35	9.17	8.22	1st vertical, aft pylon longitudinal
5	14.66	12.73	11.32	2nd vertical, pylon longitudinal
6	17.79	14.25	13.64	2nd lateral, fwd pylon lateral
7	21.38	15.19	14.83	3rd lateral, pylon lateral in phase

TAB 3. Comparison of the tuned detailed model frequencies at various weights and reduced hub mass for the NLR model

2.2. Comprehensive flight dynamics tool

The flight dynamics calculations are performed by the multi-body rotorcraft analysis and development tool Flightlab. A Boeing CH-47D Chinook simulation model has been developed, featuring a finite-element rotor blade and modal fuselage. The airframe is excited by the load transmitting hub nodes.

2.2.1. Rotor system

The dual rotor system consists of fully-articulated rotor hubs with lag dampers and three flexible blades. A six-state Peters/He wake inflow model is used. Aerodynamic interference is taken into account on both rotors (mutually) and fuselage.

The rotor blade consists of ten aerodynamic blade segments, evenly spaced along the radius. The aerodynamic properties are available through table lookup. A quasi-unsteady air loads model, based on a combination of linear unsteady thin airfoil theory and nonlinear table look-up, is used for calculating the aerodynamic loads.

The calculation time step for the rotor trims is based on 256 azimuth steps per rotor revolution to capture the high frequency content in the rotor system.

The flexible blade is modelled as a one-dimensional elastic beam. The rotor blade consists of ten structural elements. The distribution of material properties along a cross-section of the blade are condensed to a single point along the blade. The blade properties have been supplied by the Boeing Company [2]. The blade material properties have been tuned to match the frequencies by Fries [4]. The resulting blade frequencies are tabulated in TAB 4.

©DGLR 2009

Agreement with the data from literature is good.

Mode	Frequency		
	Fries [4] 230 RPM	bl. model 230 RPM	bl. model 225 RPM
1L			0.86
1F	1.02	1.02	1.02
2F	2.71	2.58	2.59
1T	4.62	4.64	4.74
3F	5.31	5.23	5.28
2L			6.40
4F			8.94
2T/5F			13.7

TAB 4. Mode and frequencies (normalised with rotor frequency)

2.2.2. Airframe model

The fuselage model is incorporated in modal form. The mass and material properties of the structural model have been gathered from data from the manufacturer and from open literature. Modal frequencies and mode shapes etc. have been generated by the dedicated structural analyses program NASTRAN. An airframe airloads model was also incorporated in the model to account for the aerodynamic loads on the fuselage. Aerodynamic coefficients are acquired by table look-up.

2.3. Fatigue life computation

The resultant calculated stress sequence in the airframe component may be fed into a fatigue load prediction tool, enabling a relative comparison of fatigue life of one airframe component for two different missions or mission elements.

3. VALIDATION

This chapter describes validation results for the models described in the previous chapter. The next section briefly describes the available experimental data. The second section compares the computational results with the experimental results for selected flight regimes. For this validation exercise only level forward flight and steady turns are considered, since they can be simulated in a relatively straightforward manner. Other regimes will show more variability, due to varying pilot input or due to currently used regime identification definitions which, in some cases, are not detailed enough.

3.1. Flight test description

Two RNLAF Chinooks have been instrumented with accelerometers and five strain gauges at different locations on the airframe. The flight parameter data has been recorded by a Combined Voice and Flight Data Recorder (CVFDR) and the ACRA KAM-500 data acquisition unit. The latter was also used to record the data from the accelerometers and strain gauges [7], [8] and [9].

Output of the strain gauges on the helicopter aft frame and accelerometers on the airframe are synchronised with the helicopter's Flight Data Recorder. A Flight Regime Recognition tool is used to process the large amount of data and to enable the selection of specified flight conditions (steady and/or manoeuvring).

A large number of scheduled operational flights have been made. For the validation exercise however a limited small number of 14 flights have been selected. Selection was based on the presence of a sufficient number of stationary, level flights at constant speed and level turns with constant bank angle. The selected flight regimes were extracted from the flight data using the NLR Flight Regime Recognition module [10].

3.2. Flight data description and processing

The strain gauge data is sampled at 512 Hz. The CVFDR data at 8Hz. FIG. 6 shows a typical graph of a performed flight and shows the time spent in Flight Regime 'level flight at 80% Vh', in red. Vh is maximum horizontal velocity. In general there will be several time intervals where the helicopter is in a given flight regime.

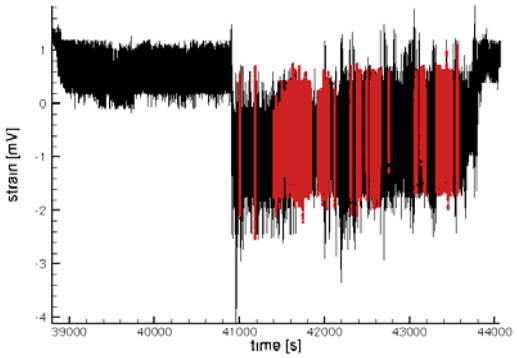

FIG. 6. Shown in red are the strain data when the helicopter is in Flight Regime 'level flight at 80% Vh'.

The 3/rev strains are extracted from the strain sequence using the classic theory of Fourier transforms. Since the Fourier transform expects the data to be periodic, it will give erroneous results on the time accumulated data. The jumps between the strain data of different time intervals will contaminate the complete Fourier spectrum, in

particular the 3/rev response. Therefore each of the time intervals is transformed separately, and a so-called Hanning window is applied to the strain data of each time interval in order to remove the error by the non-periodicity. Moreover, over each time interval a sliding window of four seconds is applied. For each window the spectrum is computed, and all the spectra of a single time interval are averaged to obtain a relatively smooth signal for the time interval under consideration.

3.3. Validation test cases

The validation focuses on the SG02 strain gauge which is positioned on the aft flange of rear pylon frame (fuselage station 482, see FIG. 9). Flight altitudes are relatively high and level flight regimes are at relatively high speeds. An overview of the flight conditions for the level flights is given in FIG. 7, for the steady turns in FIG. 8. From this figures it can be seen that the level flights are mostly flown at an altitude exceeding 6000 ft, and that the turns are mostly flown at an altitude between 4000 and 6000 ft. Also, there is limited data available for the weight class below 32000 lbm, hence the lower weight class will be ignored.

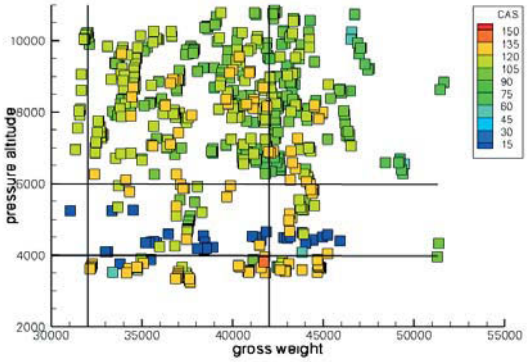

FIG. 7. Overview of the flight conditions for the level flight. Each continuous time interval for a desired flight regime is represented as a square and coloured by the calibrated air speed (CAS).

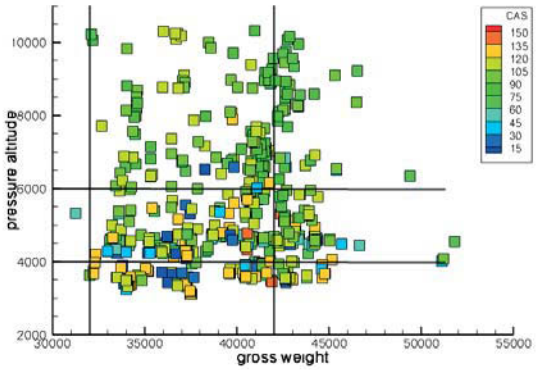

FIG. 8. Overview of the flight conditions for the steady turns. Each continuous time interval for a desired flight regime is represented as a square and coloured by the calibrated air speed (CAS).

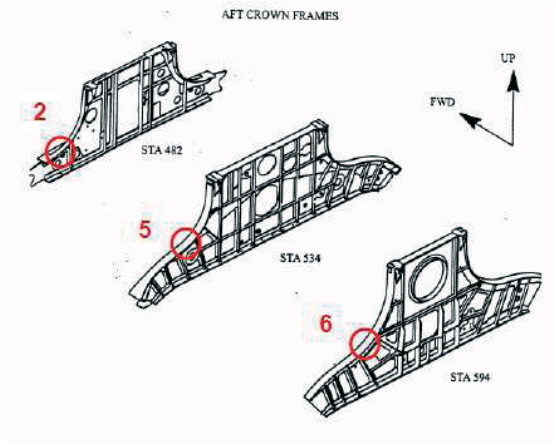

FIG. 9. Position of the strain gauges 2, 5 and 6 in the Chinook frame (from [7]). Strains from gauge 2 are used for validation in the current report.

3.4. Validation results

Simulations are conducted for level flights and turns. The level flight speed ranges from 15 to 165 knots at 15 knots intervals (10-110% of Vh). The turns concern both left and right turn at 15, 30, and 45 degrees bank angle at three different speeds: 45, 90 and 135kts.

Since it is expected that the loads will depend on gross weight and altitude, the level flights and turns will be simulated at nine different conditions: all combinations of three weights (27000, 37000, and 48000 pounds) and three pressure altitudes (1000, 5000, and 8000 ft). The experimental data is obtained from those time intervals for which the flight conditions fit the weight and altitude criteria (called a bin). The relationship between the simulated flight conditions and the bins is presented in TAB 5.

Weight [lbs]	Weight bins [lbs]	Altitude [ft]	Altitude bins [ft]
27000	up to 32000	1000	up to 4000
37000	32000-42000	5000	4000-6000
48000	from 42000 upwards	8000	from 6000 upwards

TAB 5. Relationship between simulated flight conditions and experimental bins

3.4.1. Strains for the level flights

The 3/rev vibrations and, to a lesser extent, the 6/rev vibrations, are the dominant contributors to the vibration levels so the validation focuses on the 3/rev and 6/rev strains. Note that the 1/rev strains in the flight test data is due to dissimilarities between the different rotor blades. Since the rotor blades in the simulations are identical, these 1/rev strains will not appear in the simulation.

©DGLR 2009

FIG. 10 up to FIG. 15 compares the 3/rev strain amplitudes. For some flight conditions, especially at the highest speeds combined with the highest altitudes, there are no simulation results since the computations failed to obtain a converged trim condition for the helicopter.

Overall agreement with the measurements is good. The simulations are within the scatter of the measurements. The trend in the measurements for the level flights at a gross weight of 37000 lbm and 1000 ft and 5000 ft pressure altitude (FIG. 10 and FIG. 11) which show a minimum strain level at about 100 knots is well reproduced by the simulations. For the higher speeds, it seems that the strains in the simulation are over predicted with respect to the measurements. This is analyzed in more detail in Section 3.4.2.

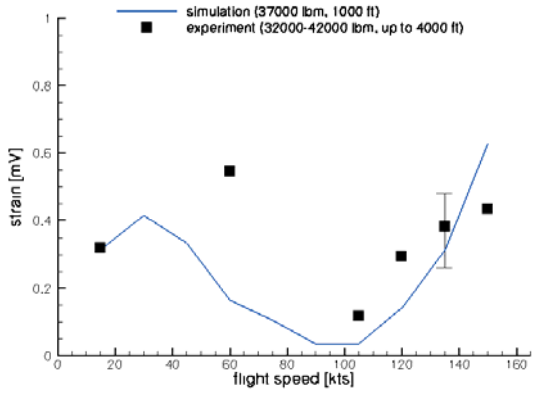

FIG. 10. Comparison between experiment (black symbols) en simulation (blue line) for level flight conditions at 1000 ft altitude and 37000 lbm gross weight. Shown is the 3/rev strain amplitude.

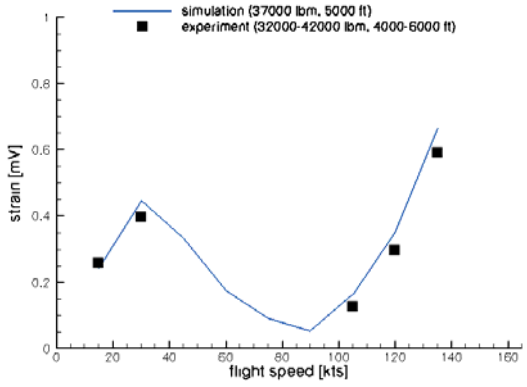

FIG. 11. Comparison between experiment (black symbols) en simulation (blue line) for level flight conditions at 5000 ft altitude and 37000 lbm gross weight. Shown is the 3/rev strain amplitude.

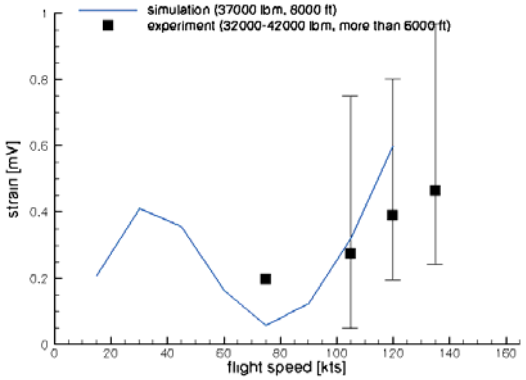

FIG. 12. Comparison between experiment (black symbols) en simulation (blue line) for level flight conditions at 8000 ft altitude and 37000 lbm gross weight. Shown is the 3/rev strain amplitude.

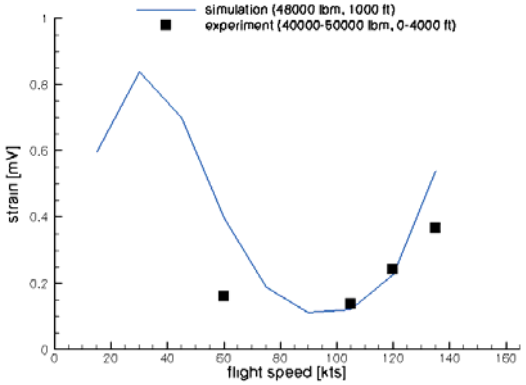

FIG. 13. Comparison between experiment (black symbols) en simulation (blue line) for level flight conditions at 1000 ft altitude and 48000 lbm gross weight. Shown is the 3/rev strain amplitude.

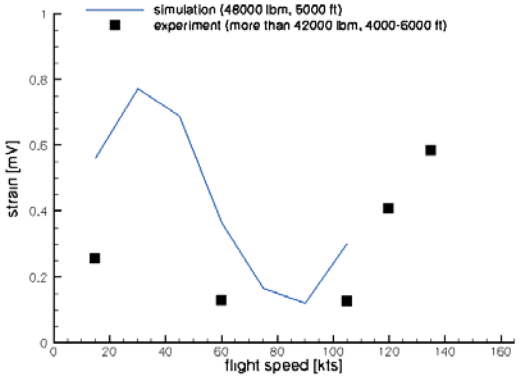

FIG. 14. Comparison between experiment (black symbols) en simulation (blue line) for level flight conditions at 5000 ft altitude and 48000 lbm gross weight. Shown is the 3/rev strain amplitude.

©DGLR 2009

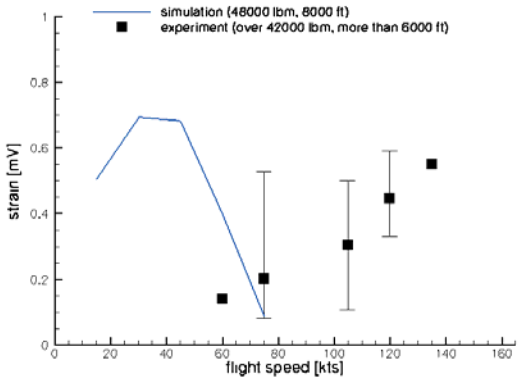

FIG. 15. Comparison between experiment (black symbols) en simulation (blue line) for level flight conditions at 8000 ft altitude and 48000 lbm gross weight. Shown is the 3/rev strain amplitude.

FIG. 16 shows a typical comparison of the 6/rev amplitudes for the level flights. The 6/rev strains are consistently under predicted by the simulations. Moreover, there is little variation in the strains with respect to the flight speed. The correct prediction of the higher frequencies is difficult to establish. Lang and Centolanza [1] showed that the predictions of the higher frequencies can be significantly improved when the fuselage motions are interpolated to a detailed component model. The strains in the simulations are computed directly from the fuselage model, so this may be one explanation of the poor prediction of the higher frequencies. Another explanation is that the fuselage mode shapes have been tuned for the lowest frequencies, but not yet for the higher frequencies.

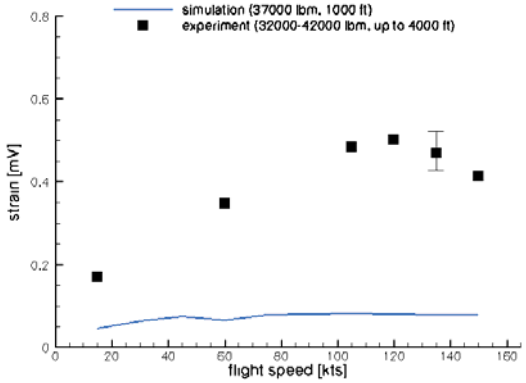

FIG. 16. Comparison between experiment (black symbols) en simulation (blue line) for level flight conditions at 1000 ft altitude and 37000 lbm gross weight. Shown is the 6/rev strain amplitude.

3.4.2. Trends analysis for the level flights

In FIG. 17 a summary of the simulation results for all level flights is presented. The 3/rev strains in the simulations show two trends: at the lower speeds the strain level mainly depends on the weight: levels increase (significantly) with increasing weight. At higher speeds (above 90 knots), the levels increase with increasing weight *and* increasing altitude. In the following, an analysis will be made to see if these trends also occur in the measurements.

FIG. 18 compares simulations and flight tests for a given weight class. The reader should be aware that some of the experimental data points are based on a limited number of samples. For the weight class of 37000 lbm, the experimental data at 1000 and 8000 ft altitude mimic the trend in the simulations: at higher speeds, an increase in altitude increases the strain levels. As the strain levels of the experiments at 5000 ft continue to increase with increasing flight speed, the strain levels for the other two altitudes seem to level off. Apparently, there is some damping effect which is not present in the simulations. For the weight class of 48000 lbm, the increase of strain levels with increasing altitude at higher speeds is repeated in the experiments. The relative insensitivity of the strain levels with respect to altitude for the lower speeds, which is seen in the simulation results, cannot be verified in the experimental results because of lack of data.

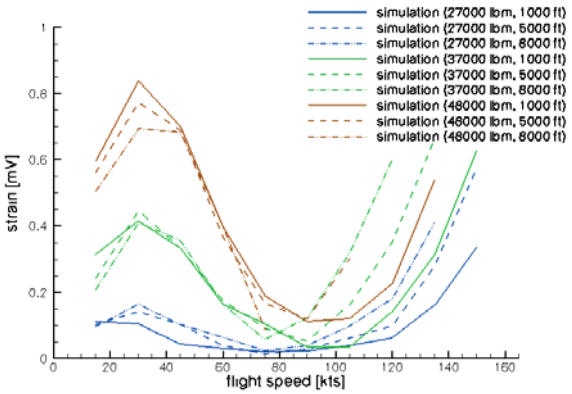

FIG. 17. Summary of the 3/rev simulation results for all level flight conditions

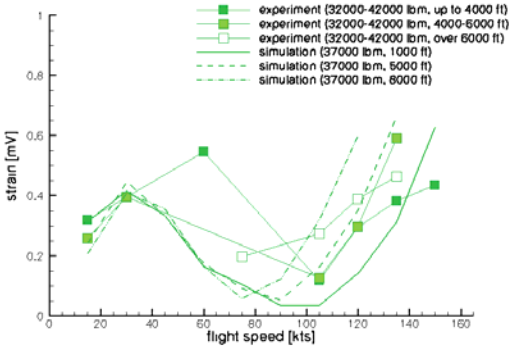

FIG. 18. Comparison of experiments (symbols) and simulations (thick lines) for the two weight classes of 37000 lbm.

3.4.3. Strains for steady turns

FIG. 19 up to FIG. 21 compares the 3/rev strain amplitudes. The number of samples for a given turn is generally small. Hence it is difficult to draw definite conclusions from the comparison with simulation results. Generally, simulation results are of the same order as the measurements. The trend of a lower strain level at 90 kts and higher levels at 45 and 135 kts is well represented.

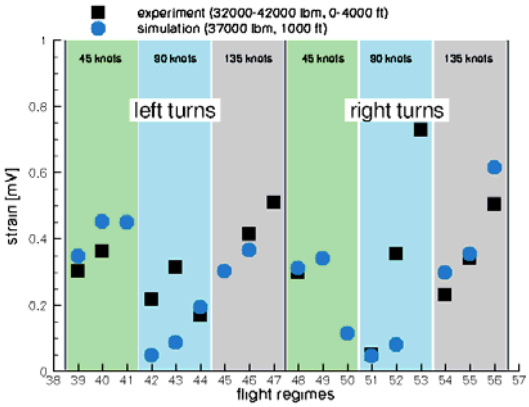

FIG. 19. Comparison between experiment (black symbols) en simulation (blue dots) for steady turns at 1000 ft altitude and 37000 lbm gross weight. Shown is the 3/rev strain amplitude. The flight regimes are consecutively numbered according to the bank angle (15, 30 and 45 degrees), flight speed (45, 90, and 135 knots) and left or right turns.

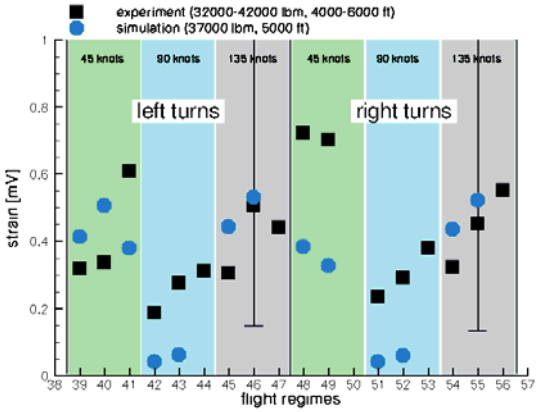

FIG. 20. Comparison between experiment (black symbols) en simulation (blue dots) for steady turns at 5000 ft altitude and 37000 lbm gross weight. Shown is the 3/rev strain amplitude. The flight regimes are consecutively numbered according to the bank angle (15, 30 and 45 degrees), flight speed (45, 90, and 135 knots) and left or right turns.

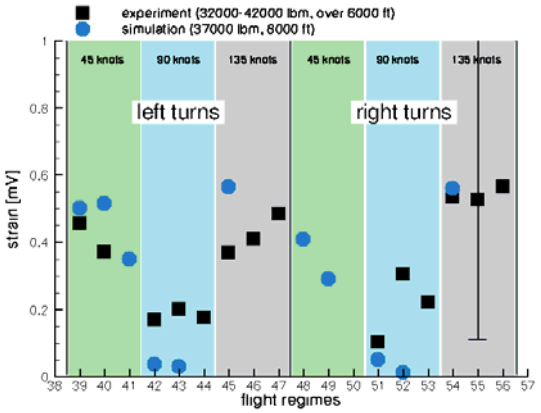

FIG. 21. Comparison between experiment (black symbols) en simulation (blue dots) for steady turns at 8000 ft altitude and 37000 lbm gross weight. Shown is the 3/rev strain amplitude. The flight regimes are consecutively numbered according to the bank angle (15, 30 and 45 degrees), flight speed (45, 90, and 135 knots) and left or right turns.

Figures FIG. 22 and FIG. 23 show typical 6/rev strains for the turns at gross weight of 37000lbm. As is the case with the level flight results, the 6/rev strain are under predicted for all turns. The number of samples for a given turn is small.

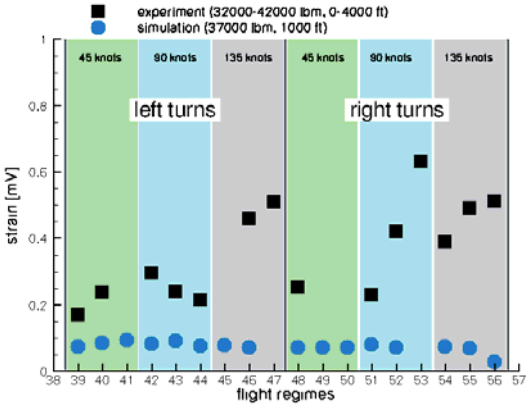

FIG. 22. Comparison between experiment (black symbols) en simulation (blue dots) for steady turns at 1000 ft altitude and 37000 lbm gross weight. Shown is the 6/rev strain amplitude. The flight regimes are consecutively numbered according to the bank angle (15, 30 and 45 degrees), flight speed (45, 90, and 135 knots) and left or right turns.

©DGLR 2009

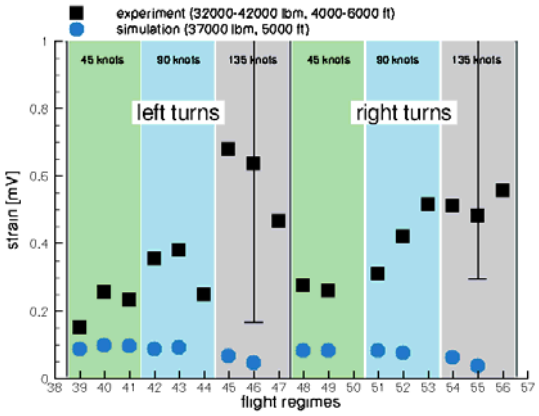

FIG. 23. Comparison between experiment (black symbols) en simulation (blue dots) for steady turns at 5000 ft altitude and 37000 lbm gross weight. Shown is the 6/rev strain amplitude. The flight regimes are consecutively numbered according to the bank angle (15, 30 and 45 degrees), flight speed (45, 90, and 135 knots) and left or right turns.

4. CONCLUSIONS

A framework for the calculation of dynamic loads in helicopter airframe components was successfully set up. A validation exercise has been executed in which the computed strain in a specific component of the airframe was compared with in-flight measurements.

The computed 3/rev strains in the aft pylon frame compare well with flight test data. The computed 6/rev strains however are consistently under predicted. Possible causes are that the fuselage model is tuned for the lowest frequencies; tuning for the higher frequencies still needs to be done. Furthermore the component model was implemented as a detailed structure integrated in the coarse fuselage model. Experience from Boeing (Lang and Centolanza [1] suggests that the use of a separate component model can improve the high-frequency response. Other causes for discrepancies are the mass and material properties of the fuselage model; the mass distribution used in the fuselage model is simplified. The airframe sheet thickness and material properties are assumed to be constant over large portions of the airframe. These assumptions are approximately correct but may differ from the actual value.

The general trend of minimal loads at medium speeds and strong increase in loads at high speeds is well captured by the simulations; for the level flights the simulations show a strong dependence on weight for the lower speeds, whereas for the higher speeds strain levels increase with both weight and height.

5. RECOMMENDATIONS

The computed strains for low flight speed and turns strains could not be validated in detail because of lack of sufficient experimental samples. Additional flights should be processed to obtain more data for a particular flight regime in order to perform a better validation and more thorough statistical analysis of the experimental data.

In order to limit the amount of data processing a rather course segmentation in weight and altitude has been used for the validation exercise. Better agreement is expected when altitude and weight bands are segmented at higher resolution.

A more detailed validation of each of the model components is required to pinpoint the origin of the discrepancies between flight test and model data.

Mass distribution and shell properties (thickness and materials) of the fuselage model should be implemented in more detail. Moreover, the position of the centre of gravity is expected to influence the overall dynamics behaviour. Tuning more individual modes of the fuselage model instead of only the first mode should also be done.

References

[1] Ph. Lang and L. Centolanza, Improved high frequency dynamic airframe loads and stress prediction, 62nd AHS Forum, Phoenix, May 9-11, 2006.
[2] DuVal, R.W., A Real-Time Mulit-Body Dynamics Architecture for Rotorcrafts Simulation, The Challenge of Realistic Rotorcraft Simulation, RAeS Conference, London, UK, November 2001
[3] The Boeing Company, A full set of blade properties (mass distribution, stiffness, elastic center offset, etc.) for the CH-47D. Private communication.
[4] J.C. Fries, The effect of structural variations on the dynamic characteristics of helicopter rotor blades, AIAA paper 90-1161-CP, 1990.
[5] R.J.J. Bakker, M.J. Bos, N. Münninghoff, J.H. van Tongeren, en H. van der Ven, Modelling framework and results for the prediction of helicopter loads for maintenance, Deliverable D2 of the NTP project HeliCompLoad, NLR-CR-2008-335, 2008.
[6] R.G Kvaternik, A government/industry summary of the design analysis methods for vibrations (DAMVIBS) Program, NASA conference publication 10114, january 1993, pages: 23-34: Boeing helicopters airframe finite element modelling by: R.Gabel, P.Lang and D.Reed, Boeing helicopters, Philadelphia, Pennsylvania
[7] M.A. Hordijk and J.A.J.A Dominicus, Installation of a loads and usage monitoring system on-board a CH-47D Chinook helicopter of the Royal Netherlands Air Force, NLR-CR-2007-044, 2007
[8] A. Oldersma, Initial analysis of the Chinook D103 testflight on April 6, 2007, Issue2, NLR-CR-2007-697, 2007
[9] A. Oldersma, Initial analysis of the Chinook D664 testflight on July 12, 2007, NLR-CR-2007-698, 2007
[10] N. Münninghof and M.F.J. Koolloos, Development of a RNLAF CH-47D Chinook Structural Integrity concept, Part 3 of 4: Feasibility study of a flight regime recognition concept for usage monitoring, NLR-CR-2004-337-PT3, 2004.
[11] The Boeing Company, Basic Mission profile for fatigue analysis. Private communication
[12] J.H. van Tongeren, R. Maas, E.G.M Geurts, RNLAF CH-47D Chinook CHASE integration, PT1 Structural

©DGLR 2009

vibration ground and flight test evaluation, NLR-CR-2007-734, Draft 2008

[13] The Boeing Company Philadelphia, Summary of airframes strain survey results R.A.F. HC Mk2a Tab No. M4454, November 1997.